ACS APPLIED MATERIALS & INTERFACES

Research Article

www.acsami.org

MC540 and Upconverting Nanocrystal Coloaded Polymeric Liposome for Near-Infrared Light-Triggered Photodynamic Therapy and Cell Fluorescent Imaging

Hanjie Wang,[†] Zhongyun Liu,[†] Sheng Wang,[†] Chunhong Dong,[†] Xiaoqun Gong,[‡] Peiqi Zhao,[§] and Jin Chang*[,†]

[†]Institute of Nanobiotechnology, School of Materials Science and Engineering, Tianjin University and Tianjin Key Laboratory of Composites and Functional Materials, Tianjin 300072, People's Republic of China

[‡]School of Life Sciences, Tianjin University, Tianjin 300072, People's Republic of China

[§]Department of Lymphoma, Tianjin Medical University Cancer Institute and Hospital, National Clinical Research Center of Cancer, Sino-US Center for Lymphoma and Leukemia, Key Laboratory of Cancer Prevention and Therapy, Tianjin 300060, China

Supporting Information

ABSTRACT: In clinic, the application of photodynamic therapy (PDT) in deep tissue is severely constrained by the limited penetration depth of visible light needed for activating the photosensitizer (PS). In this Article, a merocyanine 540 (MC540) and upconverting nanoparticle (UCN) coloaded functional polymeric liposome nanocarrier, (MC540 + UCN)/FPL, was designed and constructed successfully for solving this problem in PDT. Compared with the conventional approaches using UCNs absorbing PSs directly, the combination of UCN and polymeric liposome has unique advantages. The UCN core as a transducer can convert deep-penetrating near-infrared light to visible light for activating MC540. The functional polymeric liposome shell decorated with folate as a nanoshield can keep the UCN and MC540 stable, protect them from being attacked, and help them get into cells. The results show that (MC540 + UCN)/FPL is an individual nanosphere with an average size of 26 nm. MC540 can be activated to produce singlet oxygen successfully by upconverting fluorescence emitted from UCNs. After (MC540 + UCN)/FPL was modified with folate, the cell uptake efficiency increased obviously. More interestingly, in the PDT effect test, the (MC540 + UCN)/FPL nanocarrier further improved the inhibition effect on tumor cells by anchoring targeting folate and transactivating transduction peptide. Our data suggest that the (MC540 + UCN)/FPL nanocarrier may be a useful nanoplatform for future PDT treatment in deep-cancer therapy based on upconversion mechanism.

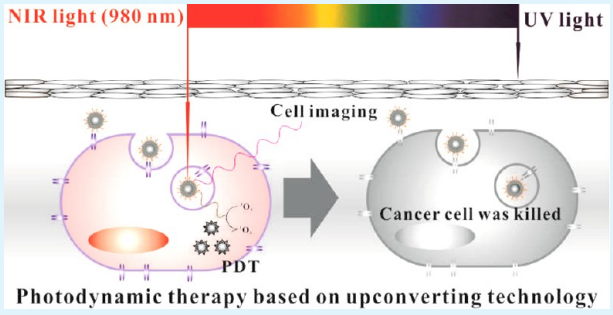

KEYWORDS: *polymeric liposome, upconverting, nanocrystal, MC540, photodynamic therapy, near-infrared light*

1. INTRODUCTION

Upconverting fluorescent nanoparticles (UCNs) emit detectable photons of higher energy in the near-infrared (NIR) or visible range upon irradiation with NIR light.[1−3] Compared to downconversion materials, UCNs have many advantages, including minimum photodamage to living organisms, low autofluorescence, high detection sensitivity, and high penetration depth in biological or environmental samples, that make them an ideal fluorescent bioimaging method for biological applications.[4−6] Among these applications, combining UCNs with photosensitizers (PSs) for photodynamic therapy (PDT) is one of the most promising fields. The NIR region is a transparent window in the tissue that can permit deeper tissue penetration than visible light.[7−9] UCNs can convert NIR light to visible photons, which can activate surrounding PSs to generate reactive oxygen species (ROS) that can kill the cancer cells. However, many problems still remain in the combination of UCNs with PSs for PDT, such as drug aggregation, drug whole-body distribution, and hard-to-penetrate membrane systems, all of which make it difficult to deliver UCNs and PSs to the deep tissue efficiently.

In recent decades, different kinds of approaches were used to overcome these problems.[10−14] Some groups loaded PSs onto $NaFY_4$-based UCNs functionalized with polymers [such as poly(ethylene glycol) (PEG), chitosan, poly(ether imide), and so on], forming a supramolecular UCNP-Ce6 complex, which is used for the NIR-light-induced PDT treatment of tumors in an animal model; some groups used mesoporous-silica-coated $NaYF_4$ upconversion to load PSs for PDT of cancer cells. Nevertheless, how to construct a multifunctional nanoplarform

Received: November 4, 2013
Accepted: February 10, 2014
Published: February 10, 2014

   dx.doi.org/10.1021/am500097f | ACS Appl. Mater. Interfaces 2014, 6, 3219−3225

for solving all of these problems and keeping a balance between the different properties is still a research hotspot in PDT based on upconverting technology.

In this work, a merocyanine 540 (MC540) and UCN coloaded functional polymeric liposome nanocarrier, (MC540 + UCN)/FPL, is developed successfully in our laboratory. The polymeric-liposome-shell-encapsulated UCNs will efficiently improve the PDT efficiency and suppress cancer cell growth. The polymeric liposome shell consists of three functionalized amphiphilic polymers: (1) octadecyl-quaternized lysine-modified chitosan (OQLCS) providing steric repulsion against particle aggregation and the ability to encapsulate PSs and UCNs;[15] (2) folate acid grafted OQLCS (FA-OQLCS) targeting the whole system to the lesions and decreasing the damage to the normal tissue;[16] (3) transactivating transduction (TAT) protein grafted OQLCS (TAT-OQLCS) having a remarkable membrane translocation capacity for helping the system to cross the membrane structures.[17]

To evaluate the performance of a (MC540 + UCN)/FPL nanocarrier, $NaYF_4$ (Y:Yb:Er = 78:20:2), UCNs and PS MC540 were all incorporated into the FPL by a reverse-phase evaporation method. The properties, such as structure, morphology, size distribution, drug loading efficiency (LE), and singlet oxygen generation in vitro, were evaluated. In addition, the targeting effect, cell uptake, and PDT treatment effect in vitro were evaluated through fluorescence microscopy and confocal laser scanning microscopy.

2. METHODS AND MATERIALS

2.1. Materials. $NaYF_4$:Yb,Er (Y:Yb:Er = 78:20:2), amphiphilic octadecyl-quaternized lysine-modified chitosan (OQLCS), targeting molecule folate acid grafted OQLCS (FA-OQLCS), and transmembrane peptide TAT-grafted OQLCS (TAT-OQLCS) were synthesized as reported in our group (details are shown in the Supporting Information). Chloroform, 9,10-anthracenediylbis-(methylene)dimalonic acid (ABDA), and merocyanine 540 (MC540) were purchased from Sigma-Aldrich. All other chemicals were of reagent grade and were used as received.

2.2. Synthesis of UCNs. $NaYF_4$ (Y:Yb:Er = 78:20:2) nanocrystals were synthesized similarly to the method reported. The details are as follows: YCl_3 (0.8 mmol), $YbCl_3$ (0.18 mmol), and $ErCl_3$ (0.02 mmol) were mixed with 6 mL of oleic acid and 15 mL of octadecene in a 50 mL flask. The solution was heated to 160 °C to form a homogeneous solution and then cooled to room temperature. A total of 10 mL of a methanol solution containing NaOH (2.5 mmol) and NH_4F (4 mmol) was slowly added to the flask and stirred for 30 min. Subsequently, the solution was slowly heated to remove methanol, degassed at 100 °C for 10 min, then heated to 300 °C, and maintained for 1 h. After the solution was cooled naturally, nanocrystals were precipitated from the solution with ethanol and washed with ethanol/water (1:1, v/v) three times.

2.3. Self-Assembly of a (MC540 + UCN)/FPL Nanocarrier. The reverse-phase evaporation method[18] was used to transfer UCNs and MC540 from the oil phase to the aqueous phase. The preparation process is shown in Figure 2. Briefly, OQLCS, TAT-OQLCS, and FA-OQLCS (weight ratio 1:1:1; total lipids 12−15 mg) were dissolved in 2 mL of water at room temperature. A 1 mL stock solution of UCNs (2 mg/mL in dichloromethane) and different volumes of MC540 were mixed with the lipid polymer solution to form an emulsion under sonication. Then, the solvents were evaporated on a rotary evaporator to form a gellike, highly concentrated suspension. After centrifugation to remove the free MC540, the (MC540 + UCN)/FPL nanocarrier suspensions were kept at 4 °C. The preparation of a (MC540 + UCN)/ PL nanocarrier without FA-OQLCS or TAT-OQLCS is the same as the method mentioned above except replacing FA-OQLCS and TAT-OQLCS with OQLCS.

2.4. Physicochemical Characterizations of a (MC540 + UCN)/FPL Nanocarrier. *2.4.1. Morphology and Particle Size Test.* The shape and morphology of the nanoparticles were measured by transmission electron microscopy (TEM) with an operating voltage of 200 kV and bright-field mode. A sample solution was dropped onto a carbon-coated copper grid and then air-dried. The effective particle size was determined by a zetasizer nano series at room temperature. About 0.2 mL of each sample suspension was diluted with 2.5 mL of water immediately after preparation.

2.4.2. Chemical Structure Test. Fourier transform infrared (FTIR) spectra were recorded with KBr pellets on an IRPrestige-21 spectrometer. A spatula full of KBr powder was added into an agate mortar and ground to a fine powder until crystallites no longer existed. Then a small amount of powder samples was taken to mix with the KBr powder. Subsequently, the mixture was ground for 3−5 min. After that, the collar together with the pellet was placed onto the sample holder.

2.4.3. Drug LE Test. The unencapsulated MC540 was collected by centrifugation, and the amount was calculated based on the UV absorbance at 540 nm. The fluorescence and UV spectrum was used to detect the emission peak strength change of different samples. The LE of the process was calculated from the following format:

$$\mathrm{LE} = (M - M_1)/(M + N) \times 100\%$$

M is the total amount of MC540 added during the preparation, M_1 is the amount of unencapsulated MC540 calculated based on the UV absorbance, and N is the total weight of the UCNs and polymers added during the preparation.

2.4.4. Singlet Oxygen Test. The generation of singlet oxygen is usually detected by singlet oxygen sensors such as ABDA. Here the ABDA method was chosen to monitor the amount of singlet oxygen. The detection of singlet oxygen production was performed through photobleaching of the chemical probe ABDA according to the previous report.[19] A mixture solution of ABDA and different samples in water was irradiated by a 980 nm laser for different times, and then the decreasing fluorescence intensity at 430 nm under excitation with 380 nm light was monitored as a function of singlet oxygen production. Photobleaching of the fluorescence emission at 430 nm can reflect the production of singlet oxygen.

2.5. Cell Study. *2.5.1. Cell Cultures.* The human breast adenocarcinoma cell line (MCF-7 cells) was used for the cell uptake test and ROS production test. MCF-7 cells were cultured in a medium supplemented with 10% (v/v) fetal bovine serum, 1% (v/v) penicillin, and streptomycin (folate free). Cells were maintained in a humidified atmosphere containing 5% CO_2.

2.5.2. Cell Uptake and ROS Production of Different Samples. Different samples with the same concentration were added to the dish, and the cells were incubated at 37 °C for 24 h. Afterward, the cells were washed three times with a phosphate-buffered saline solution. Cell imaging of the cells was performed with a laser confocal scanning microscope with an external 980 nm NIR laser. ROS generated in cells treated with different samples and then exposed to a 980 nm NIR laser detected using the ROS. Confocal images show green fluorescence indicated for ROS; the positions of the cells are indicated by red upconverting fluorescence emitted from UCNs taken up by the cells and blue fluorescence indicative of nuclear counterstaining with 4′,6-diamidino-2-phenylindole (DAPI).

2.6. PDT in Vitro. We tested the nanoparticles for their PDT efficiency in inducing cell death. MCF-7 cells were seeded onto 96-well plates and incubated for 24 h. After cell attachment, different samples were added into the wells. After culturing for 24 h, the cells in each well were exposed to 2 W/cm^2 of 980 nm NIR light for 30 min. The cell viability was measured by MTT assay.

3. RESULTS AND DISCUSSION

3.1. Formulation of a (MC540 + UCN)/FPL Nanocarrier. Most of these current PSs, such as zinc phthalocyanine (ZnPc), MC540, and so on, are only suitable for the treatment of skin disease or other superficial tissue lesions because the

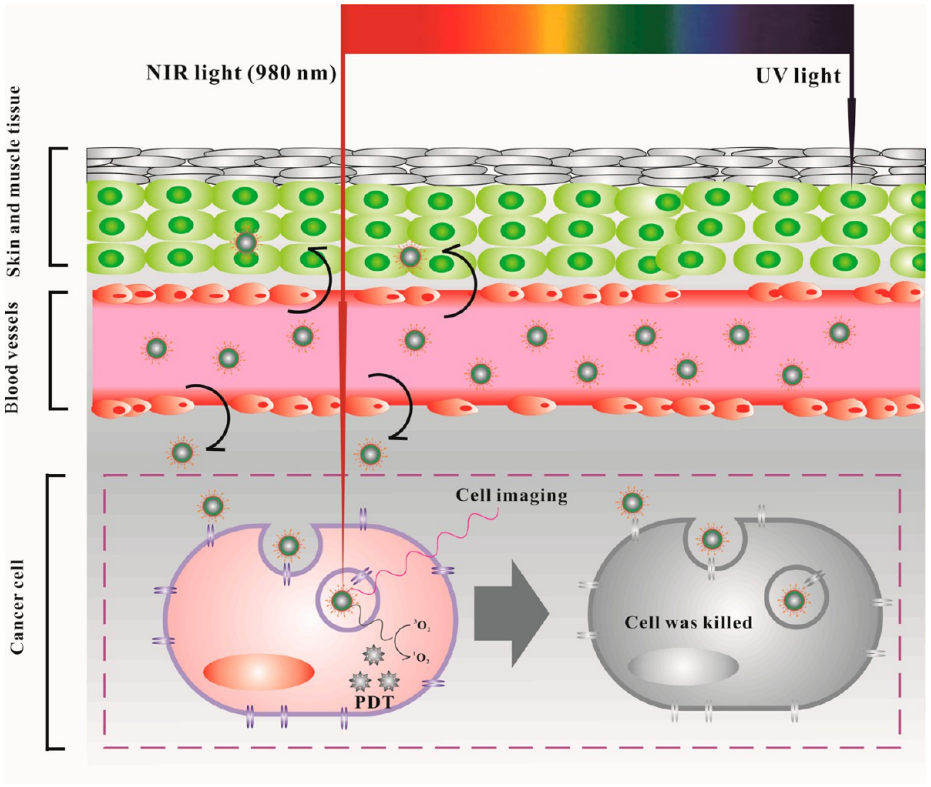

Figure 1 . Schematic illustration of PDT based on NIR-to-vis UCNs. The front part shows the penetration depth of NIR and UV light in the body tissue. The second part shows that the PS MC540 is loaded into the FPL and triggered for PDT and cell fluorescent imaging by upconverted light from NIR-to-vis UCNs.

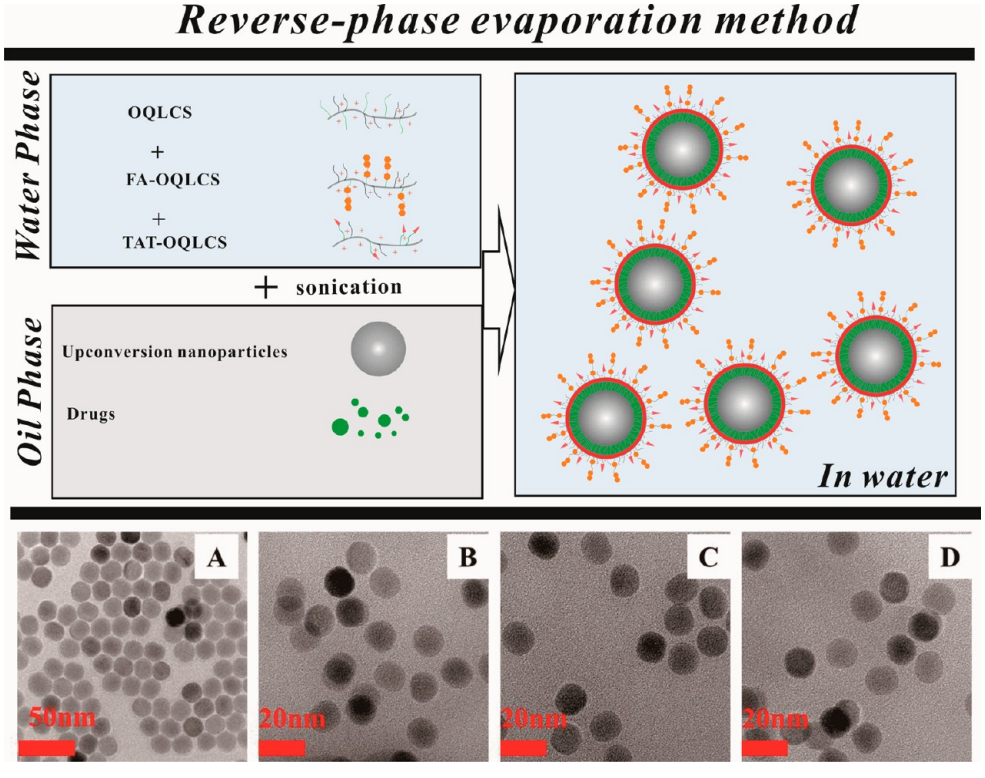

Figure 2. Reverse-phase evaporation method for the preparation of a (UCN + MC540)/FPL nanocarrier. TEM images of unmodified UCNs $NaYF_4$:Yb,Er (Y:Yb:Er = 78:20:2) (A), a UCN/PL nanocarrier (B), a UCN/FPL nanocarrier (C), and a (UCN + MC540)/FPL nanocarrier (D).

excitation light source is short wavelength. The excitation light with high energy, especially UV light, not only has a poor tissue penetration depth[20] (as shown in Figure 1) but also causes serious damage to the normal tissue, all of which make it

dx.doi.org/10.1021/am500097f | ACS Appl. Mater. Interfaces 2014, 6, 3219−3225

unacceptable for clinical use in deep tissue. NIR light has the deepest tissue penetration compared to visible and UV light. It is also safe and is expected to cause minimal photodamage to the biological specimen involved. With the help of folate targeting and TAT peptide, (MC540 + UCN)/FPL was uptaken by cells and used to transfer NIR light (980 nm) into visible light. Visible light at 540 nm emission, well-matching the absorption of MC540, was used to excite PSs to produce reactive singlet oxygen, and fluorescence at 650 nm was used for tracking the nanocarrier in vitro and in vivo, all of which can simultaneously realize imaging and PDT treatment.

3.2. Characterization of Core–Shell Nanoparticle Properties. *3.2.1. Morphology Test.* As shown in Figure 2, the reverse-phase evaporation method was used to prepare the (MC540 + UCN)/FPL nanocarrier. Briefly, polymeric lipid molecules, FA-OQLCS, OQLCS, and TAT-OQLCS, were dissolved in 2 mL of water to form the water phase. Hydrophobic UCNs and MC540 were dissolved in dichloromethane to form the organic phase. The oil phase was mixed with the water phase to form an emulsion under sonication. Then, dichloromethane in the emulsion was evaporated under high vacuum. After removal of all of the solvent, UCNs and MC540 were entrapped in the hydrophobic sections of the polymeric liposome shells. As seen in Figure 2A, the synthesized UCNs dispersed into individual ones with uniformly small sizes. On the basis of these synthesized hydrophobic UCNs, amphiphilic lipid polymers were used to transfer UCNs from organic solvent into water respectively. TEM images of UCNs surface-modified by OQLCS and functional OQLCS including TAT-OQLCS and FA-OQLCS are given in Figure 2B,C. After UCNs transferred into water, the UCNs decorated with OQLCS (Figure 2B) still dispersed as individuals with small particle sizes. Compared with UCNs modified by TAT-OQLCS and FA-OQLCS in the UCN/FPL group (Figure 2C), UCNs still remain the same size without aggregation. When MC540 was loaded into the hydrophobic interlayer between the UCN and functional polymeric lipid shell, it improved the contrast of the polymeric lipid shell. As seen in the Figure 2D inset image, a circle outside UCNs indicated that the polymeric lipid shell absorbs onto the surface of UCNs.

3.2.2. FTIR Test of the Samples. The chemical structure of a (MC540 + UCN)/FPL nanocarrier was determined by FTIR spectra. The results of FTIR analysis are shown in Figure 3. Compared with the spectrum of pure UCNs, in the spectrum of (MC540 + UCN)/PL, the appearance of new intensive peak at 1150 cm^{-1} corresponding to a C–N vibration of OQLCS and the two peaks at 2910 and 2854 cm^{-1} corresponding to methylene increased, all of which indicated that the polymeric liposome coating was successful. Compared with the spectrum of UCN/PL, in the spectrum of UCN/FPL with folate and TAT surface decoration, there are new peaks located at 1565 cm^{-1} representing NH_2 symmetric bending and 1630 cm^{-1} representing the benzene ring on folate, all of which indicated the presence of TAT peptide and folate coated on the surface of the UCN/FPL nanocarrier.

3.2.3. MC540 LE Test. The MC540 LE was defined as the weight percentage of MC540 in the whole nanocarrier, which is one of the most important parameters to evaluate the properties of a drug carrier.[21] Herein the LE of a (MC540 + UCNs)/FPL nanocarrier was studied in detail by changing the amount of MC540 added during the preparation of the nanocarrier. The same amounts of UCNs and amphiphilice

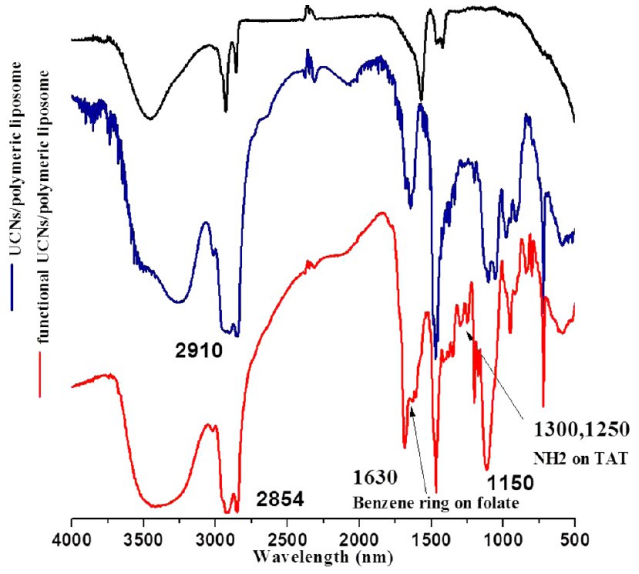

Figure 3. FTIR results of unmodified UCNs, a (UCN + MC540)/PL nanocarrier, and a (UCN + MC540)/FPL nanocarrier.

polymers were mixed with different volumes of MC540 solution (concentration: 1 mg/mL in pyridine) during the synthesis procedure. The samples were tested by UV–vis and fluorescence spectroscopy after removal of free MC540 by centrifugation and washing two times. To evidence energy transfer between UCNs and the loaded MC540, the upconverting luminescent emission spectra of a (MC540 + UCN)/FPL nanocarrier were measured. As seen in Figure 4A, with an increase of the MC540 loading, the UCL emission peak at about 540 nm became weaker and weaker, which indicated that the resonance energy transferred from UCNs to nearby MC540 molecules with an absorption peak right at 540 nm. The MC540 LE was calculated by the format between the absorbance at 540 nm and the concentration. As seen in Figure 4B, the characteristic absorption peak strength of MC540 at about 540 nm increased with an increase in the amount of MC540 loading.

Accordingly, for the absorption data, the drug LE was calculated. As shown in Figure 4C, along with an increase of MC540 added, the loading capacity is 1.7% at 10 μL of MC540 added and increased to the peak value of 9.8% at 100 μL of MC540 added. However, as seen in Figure 4D, the average particle size increased to about 140 nm when 100 μL of MC540 was added. In order to keep the balance between the LE and particle size, the amount of MC540 added was fixed at 70 μL (1 mg/mL) in the next experiment.

3.3. Detection of Singlet Oxygen Generation. An important requirement for the application of PSs in PDT is a high singlet oxygen generation efficiency. To assess the capability of singlet oxygen generation of a (MC540 + UCN)/FPL nanocarrier, ABDA was employed as a probe molecule to monitor singlet oxygen generation. In this method, ABDA can react with the newly generated singlet oxygen to yield endoperoxide, which causes a fluorescence decrease of ABDA at about 430 nm. The same amount of ABDA was added to different samples to monitor the fluorescence change. In the presence of $^1O_2$, consumption of ABDA results in fluorescence decay and provides a means of monitoring $^1O_2$ production from different samples. We measured the varying extent of ABDA decay in water in the presence of different samples. The

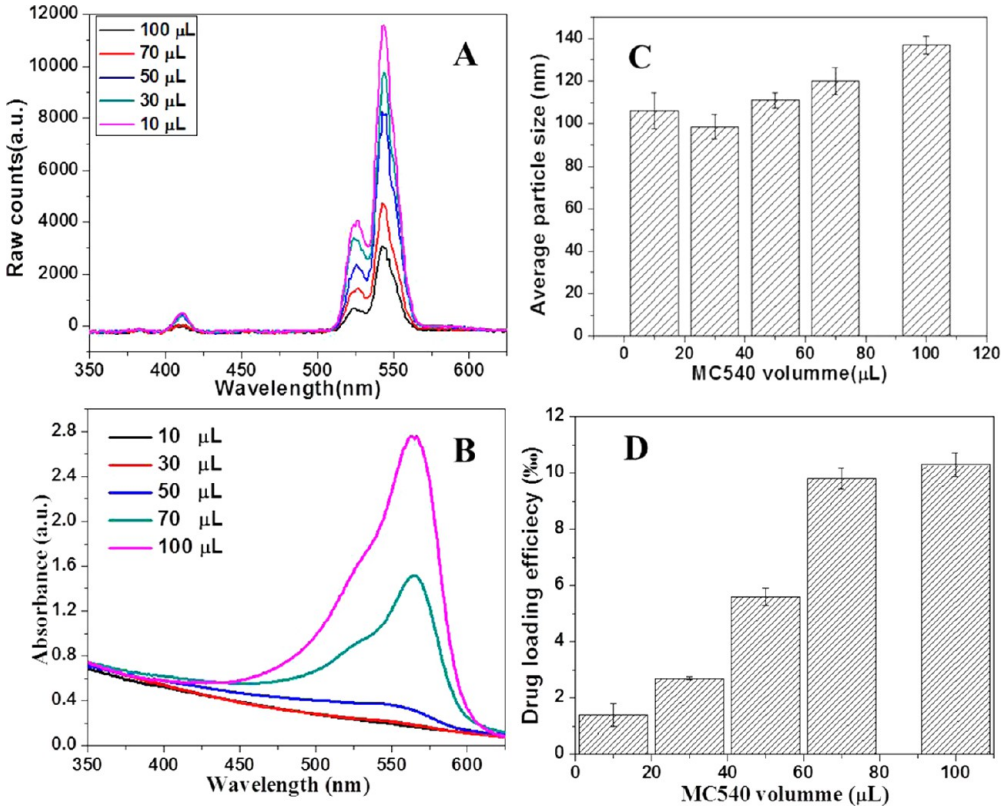

Figure 4. Fluorescence spectra (A), UV−vis spectra (B), average particle size (C), and the MC540 LE of a (UCN + MC540)/FPL nanocarrier with changes in the amount of MC540 added during the preparation (D).

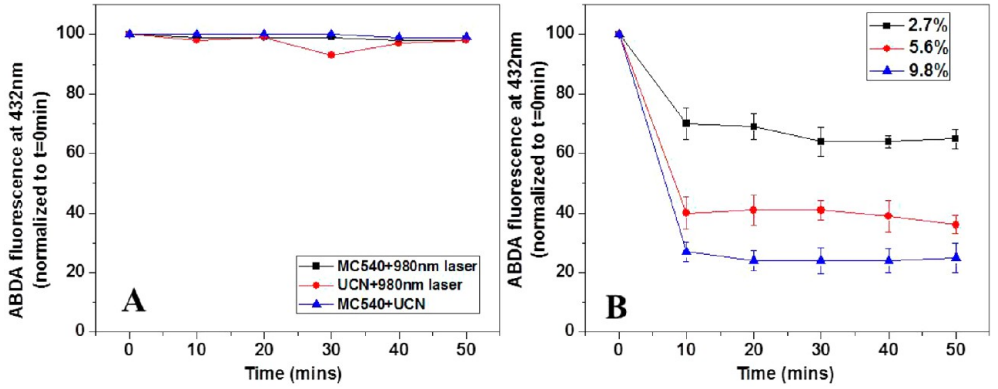

Figure 5. Comparison of $^1O_2$ production between these three experiment groups (A) and three experiment groups with different MC540 loading amounts (B), as determined by the decay of ABDA fluorescence. ABDA fluorescence decay (measured at its peak intensity at 432 nm) is plotted as a function of time (t). The percentage of the reduced fluorescence intensity of ABDA is a function of the irradiation time (the intensity was defined as 100% before light irradiation).

fluorescence spectra and decay of ABDA fluorescence of these samples are shown in Figures 5 and S5 and S6 in the SI. There are three control groups including MC540 under 980 nm laser exposure (A), UCNs under 980 nm laser exposure (B), and (MC540 + UCN)/PL without 980 nm laser exposure (C). As seen in Figure 5A, the curves show that there is nearly no decay of ABDA fluorescence with an increase of time, suggesting that there is no ROS produced in these three control groups. All of these results indicated that the UCN, MC540, and 980 nm laser exposure are dispensable for the production of ROS. The samples with different MC540 LEs (2.7%, 5.6%, and 9.8%) were used to test ROS production. As seen in Figure 5B, all of these curves show that the decay of ABDA fluorescence with an increase of time is obvious in all of these groups, and with an increase of the MC540 LE, there is much more decay of ABDA fluorescence. All of these results compared well with the control groups mentioned above.

3.4. Folate Targeting Effect Test. To confirm whether the folate decoration on the surface could improve the cell uptake efficiency, OSCC cells with a folate receptor overexpressed were used to incubate the samples with or without folate decoration.[22] The confocal images are shown in Figure 6. In the UCN/PL group (without FA-OQLCS coated), there is intensive upconverting green fluorescence emitted by UCNs, which indicated that the UCN/PL nanocarrier had been delivered into the cells. This is attributed to the polymeric

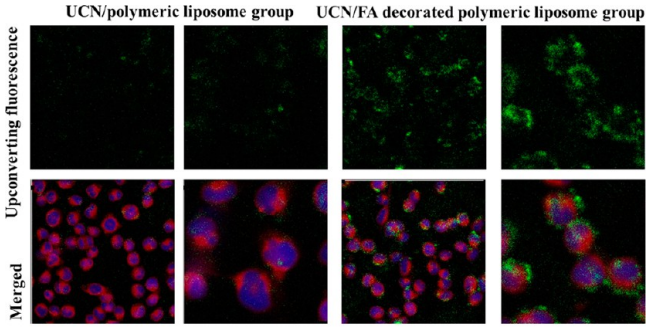

Figure 6. Folate targeting efficiency test. Confocal images showing nuclei counterstained with DAPI (blue fluorescence) and cell membrane counterstained with concanavalin A (red fluorescence) and UCNs (green fluorescence). Cells were incubated with the samples (100 μg/mL) for 30 min.

liposome shells with positive charge, which helped the nanocarrier to be uptaken by the cells. In order to further improve the cell uptake efficiency, the UCN/FPL group (with FA-OQLCS coated) was designed. After incubation, there was much stronger upconverting green fluorescence in the cells, which indicated that more UCNs were uptaken compared to UCN/PL (without FA-OQLCS coated), as is evident in Figure 6. All of these results proved that folate decoration indeed improved the cell uptake of the nanocarrier, which helped to transport more MC540 into the cells for the PDT treatment.

3.5. ROS Production in Cells. To monitor ROS production, MCF-7 cells were incubated with different samples for 24 h. In order to evaluate the ability of the UCNs to generate $^1O_2$, Image-iT Live ROS detection was used to test $^1O_2$. As seen in Figure 7, obvious red upconversion luminescence from the UCNs at 980 nm excitation and a green fluorescence ROS marker were simultaneously observed in the cancer cells. The merged images indicate that fluorescence of UCNs and green fluorescence of a ROS marker coexist in the cells, mainly appearing in the cytoplasmic regions.

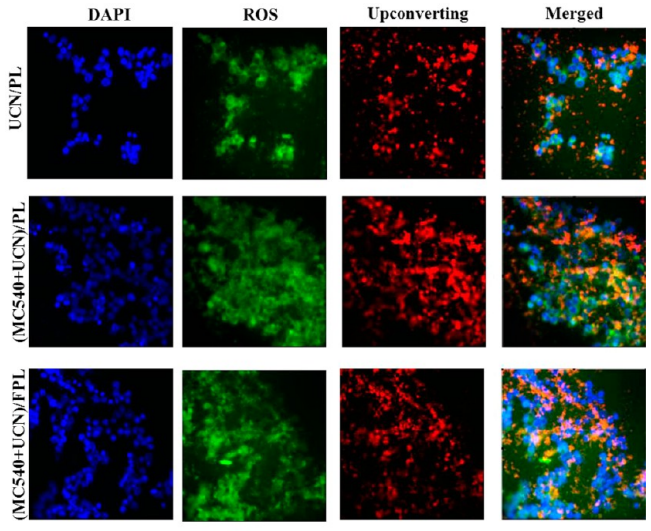

Figure 7. ROS production test in cells. Confocal images showing nuclei counterstained with DAPI (blue fluorescence) and cells labeled with carboxy-H2DCFDA that fluorescence when oxidized in the presence of reduced oxygen species (green fluorescence) and UCNs (red fluorescence).

Compared with the UCN/PL group without loaded MC540, there was much stronger green fluorescence in the (MC540 + UCN)/PL group, which proved that the energy emitted from UCNs at 980 nm excitation successfully transferred to MC540.

TAT peptide is a regulatory protein that drastically enhances the efficiency of viral transcription, which can be modified on the surface of nanoparticles to help them to cross the membrane structure in the body. So, in order to further improve the cell uptake efficiency, TAT-OQLCS and FA-OQLCS were mixed with OQLCS to form the lipid micelle, which was coated on the surface of UCNs to form the (UCN + MC540)/FPL group. As seen in Figure 8, the green

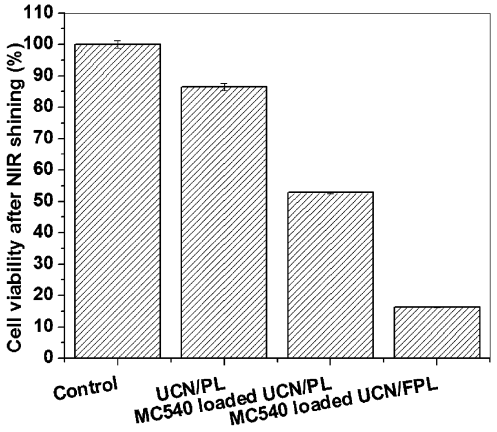

Figure 8. Efficacy of the PDT treatment of blank cells (control group), UCN/PL with NIR shining, (MC540 + UCN)/PL with NIR shining, and folate- and TAT-decorated (MC540 + UCN)/PL [(MC540 + UCN)/FPL group] with NIR shining.

fluorescence of the ROS marker and the red fluorescence of UCNs in the (UCN + MC540)/FPL group were more intense than that of cells treated with (UCN + MC540)/PL without TAT and folate, which indicated more ROS production in the cells with the help of targeting ligand folate and TAT.

3.6. PDT Effects on cancer cells. The ultimate goal for PDT treatment in this research is to kill the cancer cells in vitro. So, the efficacy of the PDT treatment (by exposing cells to a 980 nm laser for 30 min) was assessed by measuring the cell viability using MTT assay. Because MC540 can be successfully excited by the high-energy photon emitted from UCN and produces singlet oxygen for inducing cell death, in order to further improve the PDT efficiency, (MC540 + UCN)/FPL with folate and TAT decoration was designed. As seen in Figure 8, after 30 min of shining with a 980 nm laser, the cell viability is 35% in a MC540-loaded UCN/PEG-OQPGA group, which is lower than that in a UCN/PEG group without MC540 loading. These results implied that UCNs has an increased treatment effect after being combined with the PS MC540. Similarly, there was only 16.3% cell viability in the (UCN + MC540)/FPL group, which confirmed that targeting modification on the surface of a nanocarrier greatly increased the PDT efficiency.

4. CONCLUSIONS

In summary, (MC540 + UCN)/FPL, as new PS carriers for PDT, was prepared successfully via a reverse-phase evaporation method. It has been demonstrated that these nanocarriers have nanosize and narrow-size distribution. Hydrophobic MC540

can be loaded into the nanocarrier through hydrophobic interactions. The cell uptake results suggested that the fluorescence emitted from UCNs excited by NIR can effectively activate the PS MC540 to generate cytotoxic ROS. In the PDT test, the (MC540 + UCN)/FPL group modified with folate and TAT has much better treatment effect in the tumor cells. In conclusion, the UCN/lipid micelle nanoparticle may be suitable as a potential drug-delivery system for PDT based on the upconverting mechanism.

■ ASSOCIATED CONTENT

Supporting Information

Detailed methodology and experimental results. This material is available free of charge via the Internet at http://pubs.acs.org.

■ AUTHOR INFORMATION

Corresponding Author

*E-mail: jinchang@tju.edu.cn.

Notes

The authors declare no competing financial interest.

■ ACKNOWLEDGMENTS

The authors gratefully acknowledge the National Natural Science Foundation of China (Grants 51303126, 51373117, and 81070871) and Key Project of Tianjin Natural Science Foundation (Grant 13JCZDJC33200).

■ REFERENCES

(1) Challenor, M.; Gong, P.; Lorenser, D.; Fitzgerald, M.; Dunlop, S.; Sampson, D. D.; Iyer, K. S. Iron Oxide-Induced Thermal Effects on Solid-State Upconversion Emissions in NaYF4:Yb,Er Nanocrystals. *ACS Appl. Mater. Interfaces* **2013**, *5*, 7875−7880.

(2) Shen, J.; Zhao, L.; Han, G. Lanthanide-doped Upconverting Luminescent Nanoparticle Platforms for Optical Imaging-Guided Drug Delivery and Therapy. *Adv. Drug Delivery Rev.* **2013**, *65*, 744−755.

(3) He, X.; Wang, K.; Cheng, Z. In vivo Near-infrared Fluorescence Imaging of Cancer with Nanoparticle-based Probes. *Wiley Interdiscip. Rev. Nanomed. Nanobiotechnol.* **2010**, *2*, 349−366.

(4) Peng, J.; Sun, Y.; Zhao, L.; Wu, Y.; Feng, W.; Gao, Y.; Li, F. Polyphosphoric Acid Capping Radioactive/Upconverting NaLuF4:Yb,Tm,(153)Sm nanoparticles for blood pool imaging invivo. *Biomaterials* **2013**, *34*, 9535−44.

(5) Wang, C.; Cheng, L.; Liu, Z. Upconversion Nanoparticles for Photodynamic Therapy and Other Cancer Therapeutics. *Theranostics* **2013**, *3*, 317−330.

(6) Idris, N. M.; Gnanasammandhan, M. K.; Zhang, J.; Ho, P. C.; Mahendran, R.; Zhang, Y. In Vivo Photodynamic Therapy using Upconversion Nanoparticles as Remote-controlled Nanotransducers. *Nat. Med.* **2012**, *18*, 1580−U190.

(7) Mitsunaga, M.; Ogawa, M.; Kosaka, N.; Rosenblum, L. T.; Choyke, P. L.; Kobayashi, H. Cancer Cell-selective in Vivo near Infrared Photoimmunotherapy Targeting Specific Membrane Molecules. *Nat. Med.* **2011**, *17*, 1685−1691.

(8) Kumar, R.; Ohulchanskyy, T. Y.; Roy, I.; Gupta, S. K.; Borek, C.; Thompson, M. E.; Prasad, P. N. Near-Infrared Phosphorescent Polymeric Nanomicelles: Efficient Optical Probes for Tumor Imaging and Detection. *ACS Appl. Mater. Interfaces* **2009**, *1*, 1474−1481.

(9) Liu, J.; Bu, W.; Pan, L.; Shi, J. NIR-Triggered Anticancer Drug Delivery by Upconverting Nanoparticles with Integrated Azobenzene-Modified Mesoporous Silica. *Angew. Chem., Int. Ed.* **2013**, *52*, 4375−4379.

(10) Chatterjee, D. K.; Gnanasammandhan, M. K.; Zhang, Y. Small Upconverting Fluorescent Nanoparticles for Biomedical Applications. *Small* **2010**, *6*, 2781−2795.

(11) Ang, L. Y.; Lim, M. E.; Ong, L. C.; Zhang, Y. Applications of upconversion nanoparticles in imaging, detection and therapy. *Nanomedicine* **2011**, *6*, 1273−1288.

(12) Lin, M.; Zhao, Y.; Wang, S.; Liu, M.; Duan, Z.; Chen, Y.; Li, F.; Xu, F.; Lu, T. Recent Advances in Synthesis and Surface Modification of Lanthanide-doped Upconversion Nanoparticles for Biomedical Applications. *Biotechnol. Adv.* **2012**, *30*, 1551−1561.

(13) Cheng, L.; Wang, C.; Liu, Z. Upconversion Nanoparticles and Their Composite Nanostructures for Biomedical Imaging and Cancer Therapy. *Nanoscale* **2013**, *5*, 23−37.

(14) Shen, J.; Zhao, L.; Han, G. Lanthanide-doped Upconverting Luminescent Nanoparticle Platforms for Optical Imaging-guided Drug Delivery and Therapy. *Adv. Drug Delivery Rev.* **2013**, *65*, 744−755.

(15) Wang, H. J.; Zhao, P. Q.; Su, W. Y.; Wang, S.; Liao, Z. Y.; Niu, R. F.; Chang, J. PLGA/Polymeric Liposome for Targeted Drug and Gene Co-delivery. *Biomaterials* **2010**, *31*, 8741−8748.

(16) Wang, H. J.; Zhao, P. Q.; Liang, X. F.; Gong, X. Q.; Song, T.; Niu, R. F.; Chang, J. Folate-PEG Coated Cationic Modified Chitosan - Cholesterol Liposomes for Tumor-targeted Drug Delivery. *Biomaterials* **2010**, *31*, 4129−4138.

(17) Wang, H. J.; Zhang, S. N.; Liao, Z. Y.; Wang, C. Y.; Liu, Y.; Feng, S. Q.; Jiang, X. G.; Chang, J. PEGlated Magnetic Polymeric Liposome Anchored with TAT for Delivery of Drugs Across the Blood-spinal Cord Barrier. *Biomaterials* **2010**, *31*, 6589−6596.

(18) Liang, X. F.; Wang, H. J.; Luo, H.; Tian, H.; Zhang, B. B.; Hao, L. J.; Teng, J. I.; Chang, J. Characterization of Novel Multifunctional Cationic Polymeric Liposomes Formed from Octadecyl Quaternized Carboxymethyl Chitosan/Cholesterol and Drug Encapsulation. *Langmuir* **2008**, *24*, 7147−7153.

(19) Wang, X.; Zhang, Q.; Zhao, J.; Dai, J. One-step Self-assembly of ZnPc/NaGdF4:Yb,Er Nanoclusters for Simultaneous Fluorescence Imaging and Photodynamic Effects on Cancer Cells. *J. Mater. Chem. B* **2013**, *1*, 4637−4643.

(20) Yano, S.; Hirohara, S.; Obata, M.; Hagiya, Y.; Ogura, S.; Ikeda, A.; Kataoka, H.; Tanaka, M.; Joh, T. Current States and Future Views in Photodynamic Therapy. *J. Photochem. Photobiol. C* **2011**, *12*, 46−67.

(21) Kim, S.; Shi, Y.; Kim, J. Y.; Park, K.; Cheng, J.-X. Overcoming the Barriers in Micellar Drug Delivery: Loading Efficiency, in Vivo Stability, and Micelle-cell Interaction. *Expert Opin. Drug Discovery* **2010**, *7*, 49−62.

(22) Chiu, S. J.; Marcucci, G.; Lee, R. J. Efficient Delivery of an Antisense Oligodeoxyribonucleotide Formulated in Folate Receptor-targeted Liposomes. *Anticancer Res.* **2006**, *26*, 1049−1056.